Available online at www.sciencedirect.com
ScienceDirect
International Journal of Multiphase Flow 32 (2006) 1100–1109
International Journal of Multiphase Flow
www.elsevier.com/locate/ijmulflow

On the nonlinear stability of a swirling liquid jet

Hongbok Park [a], Sam S. Yoon [b,*], Stephen D. Heister [a]

[a] School of Aeronautics and Astronautics, Purdue University, 315 N. Grant Street, W. Lafayette, IN 47907, USA
[b] Department of Mechanical Engineering, Korea University, Anam-dong, 5-Ga, Sungbuk-gu, Seoul 136-713, Republic of Korea

Received 4 November 2005; received in revised form 4 May 2006

Abstract

The nonlinear deformation and atomization of a rotating column is considered using an axisymmetric boundary element formulation. Swirl has been considered by superposing a potential vortex to the bulk flow of the jet. The resulting model has been shown to reproduce the classical linear result due to Ponstein and parametric studies are conducted in the nonlinear regime to determine wave shapes and droplet sizes. As with prior nonlinear column breakup studies, results indicate that satellite drops are formed from the main wave under virtually all conditions. The ratio of the main drop to satellite drop diameter is shown to be remarkably constant over a variety of wave numbers/column lengths thereby providing a potential approach to produce tightly controlled bimodal sprays.

Keywords: Atomization; Drop size; Liquid jet; Instability; Swirl

1. Introduction

The instability of a jet is of significant interest in both the academic community and within industries due to the wealth of practical industrial applications including: ink-jet printing, agricultural sprays, IC-engines, and numerous manufacturing and painting processes. If drop size is to be predicted using the instability theory, the predicted value can be of great value as an initial condition for a spray simulation and as validation data when designing a spray nozzle for a specific application.

The origins of the instability theory can date back to the late eighteenth century by the Lord Rayleigh (1878). The Rayleigh's inviscid incompressible column jet analysis is probably the most classical and most frequently cited linear instability theory in the relevant literature. Weber (1931) extended Rayleigh's analysis by adding the effect of viscosity of the jet. It is note worthy that both Rayleigh (1878) and Weber (1931) considered the limiting case of $ka \to 0$ (where k is the wavenumber and a is the column jet radius), which indicates that the both analyses are applicable for the relatively large wavelength only; the wavelength is greater or

* Corresponding author. Tel.: +82 2 3290 3376; fax: +82 2 926 9290.
E-mail address: skyoon@korea.ac.kr (S.S. Yoon).

0301-9322/$ - see front matter © 2006 Elsevier Ltd. All rights reserved.
doi:10.1016/j.ijmultiphaseflow.2006.05.002

comparable to the jet radius). The linear theories were later revisited by Levich (1962), Sterling and Sleicher (1975), and Reitz and Bracco (1982). Their linear theories are applicable for the viscous jet and for a wide range of wavenumber. However, all the linear theories are limited to the case of infinitesimal deformation and therefore cannot strictly be used to predict droplet sizes.

It is now well known that the nonlinearity in the surface deformation process produces several satellite drops as multiple crests are formed over a given wave on the free surface. In this case, the linear theory cannot predict the satellite drop formation. Yuen (1968) extended the Rayleigh's linear theory to the nonlinear case, where Yuen derived the lengthy 2nd and the 3rd order terms for the dispersion equation. Yuen's theory was later validated with the experimental data of Rutland and Jameson (1970). However, it was later pointed out, by Nayfeh (1970), that Yuen's 3rd order terms was incorrect for the wavenumbers close to the cutoff wavenumber. Lafrance (1975) provided the correct 3rd order term in analytic form, which was free from the secular terms contained in the Yuen's analysis. More recently, a nonlinear unsteady calculation was achieved numerically using the boundary element method (BEM) for the column jet by Hilbing and Heister (1996). They validated their predicted satellite drop size with the experimental data of Rutland and Jameson and then showed the controlling mechanism for drop size. Surely, both theoretical and numerical analyses for both linear and nonlinear cases are well archived for a column jet in the literature. However, the instability study on the effect of swirl (or rotation) on a column jet has been studied less.

It appears that Ponstein (1959) is the first author who considered the effect of swirl on the stability of a classical liquid jet/column. The Ponstein's analysis was so complete and original that Ponstein's dispersion equation is capable of recovering the dispersion equations of the aforementioned authors (Rayleigh, 1878; Weber, 1931; Levich, 1962; Reitz and Bracco, 1982) for their specific cases when considering the non-swirling case. The Ponstein's equation can also recover the Kelvin–Helmoltz and the Taylor's equation for the limiting case of $ka \to \infty$, where the relevant wavelengths are much smaller than the jet diameter. Ibrahim (1993) solved one dimensional unsteady Navier–Stokes equations applied for the swirling jet and showed his numerical solutions were in agreement with the Ponstein's linear theory. Ibrahim later included the convective term and presented the nonlinear results. The nonlinear result indicated that the growth rate was a bit smaller than that of the linear result. No shift in the wavenumber of the maximum growth rate was clearly observed and, thus, the information on the reduction of the main drop size due to the mass loss to the satellite drops could not be obtained.

It is our objective to extend the linear theory and prior nonlinear results in order to identify the presence of, and size of, any satellite droplets formed during the nonlinear portion of the jet deformation. The presence of satellite droplets has long been noted in the Rayleigh jet (Lundgren and Mansour, 1988; Hilbing and Heister, 1996), and today nonlinear simulations can reproduce the measured droplet sizes quite accurately. While electrostatics (Setiawan and Heister, 1997) and jet excitation (Orme and Muntz, 1990) have been used in the past to control droplet sizes in the Rayleigh regime, the use of swirl has not been studied in any detail. Here we employ an axisymmetric boundary element method (BEM) by superposing a potential vortex with the bulk mean flow. The computations are validated against Ponstein's linear theory and parametric studies are reported for the nonlinear case.

2. Model development

Since the early 1990s, boundary element method (BEM) solutions have appeared in the literature for atomization problems of various types. Solutions for the classical liquid jet (Lundgren and Mansour, 1988), the finite-length liquid jet (Hilbing and Heister, 1996), electrostatic jets (Setiawan and Heister, 1997), and jets in wind-induced regimes (Spanger et al., 1995) have provided nonlinear companions to classical linear results dating back to Rayleigh's classic work in the late 1800s. In case of non-swirling flow, Yoon and Heister (2004) provide a complete description of the basic model elements while the complete modeling description can be found in Park and Heister (2006) for a swirling flow. For that reason, only highlights will be presented here in the interest of brevity. The addition of a capability to consider swirling flows was required for this application, and this treatment will be discussed in detail.

An inviscid, incompressible, axisymmetric flow is presumed such that the flow dynamics are governed by Laplace's equation, $\nabla^2\phi = 0$, where ϕ is the velocity potential. The BEM utilizes an integral representation

of this equation to provide a connection between ϕ values on the boundary, the local geometry, and the local velocity normal to the boundary, $q = \partial\phi/\partial n$, as follows:

$$\alpha\phi(\vec{r}_i) + \int_S \left[\phi\frac{\partial G}{\partial \hat{n}} - qG\right] \mathrm{d}s = 0 \tag{1}$$

where $\phi(\vec{r}_i)$ is the value of the potential at a point $\vec{r}_i$, S is the boundary of the domain, α is the singular contribution when the integral path passes over the "base point", and G is the free space Green's function corresponding to Laplace's equation. For an axisymmetric domain, the free space Green's function can be expressed in terms of elliptic integrals of the first and second kinds and is a function solely of the instantaneous surface geometry. For this reason, a discrete representation of Eq. (1) can be cast as a linear system of equations relating local ϕ and q values. In the discretization, both ϕ and q are assumed to vary linearly along each element, thereby providing formal second-order accuracy for the method. Since the resulting integrals do not have exact solutions in this case, Gaussian quadrature (Smirnov, 1964) is used to maintain high accuracy of integration and preserve second-order accuracy overall.

While this governing equation is linear, nonlinearities in these free surface problems enter through the boundary condition at the interface. The unsteady Bernoulli equation provides a connection between the local velocity potential and the surface shape at any instant in time. Prior formulations (Yoon and Heister, 2004; Park et al., 2005; Park and Heister, 2006) have provided a derivation of this result suitable for implementation in a Lagrangian surface tracking environment. For the swirling flow, modifications are required to account for the centrifugal pressure gradient created by the swirl. Assuming we have a coordinate system moving with the bulk velocity of the jet, the dimensional capillary velocity, $U = (\sigma/\rho a)^{1/2}$, is the velocity chosen for the nondimensionalization; the Weber number becomes a unity in this case. Using this quantity, the dimensional jet radius (a), and the liquid density (ρ), the unsteady dimensionless Bernoulli equation without swirl is as follows:

$$\frac{\mathrm{D}\phi^*}{\mathrm{D}t^*} = \frac{1}{2}|\vec{u}_t^*|^2 - \vec{u}_t^* \cdot \vec{u}_v^* - P_{\mathrm{g}}^* - \kappa + Boz^* \tag{2}$$

where z^* is the axial coordinate, P_{g}^* is the imposed gas pressure, capillary forces are accounted for via the local surface curvature, κ, and the Bond number ($Bo = \rho g a^2/\sigma$) addresses any hydrostatic pressure changes. Physically, this result is a Lagrangian form suitable for use for fluid elements moving with the local velocity of the free surface.

The total surface velocity, $\vec{u}_t$, can be computed via a superposition of the base axial flow in the injector $(\phi, \vec{u})$ with a potential vortex $(\phi_v, \vec{u}_v)$. Letting u, v, w represent axial, radial, and circumferential velocity components respectively, we may write

$$\phi_t = \phi + \phi_v, \quad u_t = u + u_v, \quad v_t = v + v_v, \quad w_t = w + w_v \tag{3}$$

Superposition of a potential vortex can be achieved by starting with the complex potential

$$F(z) = -\frac{\mathrm{i}\Gamma}{2\pi}\log(z) \tag{4}$$

It is noted that z is complex variable herein, Γ is vortex strength, and F is the complex potential.

The resulting velocity components for this flow are as follows:

$$u_v = 0, \quad v_v = 0, \quad w_v = \frac{\Gamma}{2\pi r} \tag{5}$$

This vortex is irrotational everywhere except at $\vec{r} = 0$. Using Eq. (5), the total velocity in Eq. (3) can be computed;

$$\frac{1}{2}|\vec{u}_t|^2 - \vec{u}_t \cdot \vec{u}_v = \frac{1}{2}(u^2 + v^2 - w_v^2) \tag{6}$$

where

$$\frac{1}{2}w_v^2 = \frac{1}{2}\left(\frac{\Gamma}{2\pi r}\right)^2 = \frac{1}{2}\left(\frac{2\pi a U_{\mathrm{s}}}{2\pi r}\right)^2 = \frac{1}{2}\left(\frac{a U_{\mathrm{s}}}{r}\right)^2 \tag{7}$$

It is noted that U_s is the swirling velocity of the jet at its surface, i.e. where $r = a$. Nondimensionalizing this result using the approach described above gives:

$$\frac{D\phi^*}{Dt^*} = \frac{1}{2}\left|\vec{u}^*\right|^2 - P_g^* - \kappa + Boz^* - \frac{1}{2Ro^2 r^{*2}} \tag{8}$$

Here the Bond numbers is defined above and Rossby number is defined as the ratio of capillary velocities and swirling: $Ro = (\sigma/\rho a)^{1/2}/U_s$. Thus if swirling increases (U_s), then Ro decreases, and vice versa. In this modified Bernoulli equation accounting for the swirl velocity, the last term on the RHS of the equation corresponds to the circumferential pressure developed by the potential vortex. For the present simulations we neglect gravity and the interactions with the gas phase $P_g^* = Bo = 0$.

To determine the evolution of the free surface with time, a Lagrangian form of the kinematic condition is utilized:

$$\frac{Dz}{Dt} = \frac{\partial\phi}{\partial s}\cos\beta - q\sin\beta \quad \frac{Dr}{Dt} = \frac{\partial\phi}{\partial s}\sin\beta + q\cos\beta \tag{9}$$

where β is the local slope of the wave with respect to the horizontal direction. Eqs. (8) and (9) are integrated in time using a 4th-order Runge–Kutta scheme to provide the evolution of the velocity potential and the motion of the free surface.

For long integrations or resolution of highly distorted surfaces, points on the free surface will tend to bunch in regions of higher curvature as a result of the free-surface motion. For this reason, the points on the free surface are redistributed at each time step using a cubic spline fitting (Yoon and Heister, 2004) of the instantaneous shape. The Laplace equation is solved to update velocities and the process is marched forward in time. Formally, the resolution of the scheme is second-order in space and 4th-order in time, but surface curvature and capillary forces are resolved with 4th-order accuracy given a set of points defining the instantaneous shape. More details regarding the numerical procedure can be found in Hilbing and Heister (1996).

Ponstein (1959) was the first author to consider the linear stability of the swirling jet. Presuming that the deformation of the surface from a cylindrical shape takes the form of $\eta = \eta_0 e^{(\varpi t + ikz)}$ for an infinitesimal disturbance, his classic result relates the growth rate, ω, to the wave number of that disturbance, k, as follows:

$$\omega^2 = \left[\frac{\sigma}{\rho a^3}(1 - k^2a^2) + \left(\frac{\Gamma}{2\pi a^2}\right)^2\right](ka)\frac{I_1(ka)}{I_0(ka)} \tag{10}$$

where I_0 and I_1 are modified Bessel functions of the zeroth and 1st order, respectively. When $\Gamma = 0$ (equivalent to $Ro \to \infty$ or $U_s \to 0$), this result reduces to the classic Rayleigh result for instability of a liquid column.

3. Results and discussion

Fig. 1 shows the computational domain for the rotating infinite liquid jet in this simulation. A constant grid spacing of $ds^* = 0.005$ along the liquid surface was employed for this calculation. Thus total number of grid points is dependent on the investigated wave length; typical grids employed vary from 100 to 400 nodes in the simulations. The calculated result was compared against the linear result given by Eq. (10) by running a series of calculations at different k and Ro values. Assuming a very small initial deflection, $\eta_0^* = 0.0001$, and time step, $dt^* = 0.0025$, the growth rate was computed from the numerical result using surface velocities, which was derived by Lundgren and Mansour (1988).

$$\omega^{*2} = \frac{v_r^{*2}}{(r^* - 1)^* - \eta_0^{*2}} \tag{11}$$

where $v_r^* = dr^*/dt^*$. At the peaks ($kz = 0,\ 2\pi$) and trough ($kz = \pi$) of the wavelength, the normal velocity obtained by the BEM solver can be utilized directly in the calculation. Fig. 2 shows the growth rate of the liquid jet as a function of dimensionless simulation time. The computational time to get the converged growth rate varies slightly according to the flow conditions, i.e. wave number and Rossby number. However the growth rate in most of simulations was quickly converged in 30 minutes on the 1.0 GHz Athlon CPU used in the modeling.

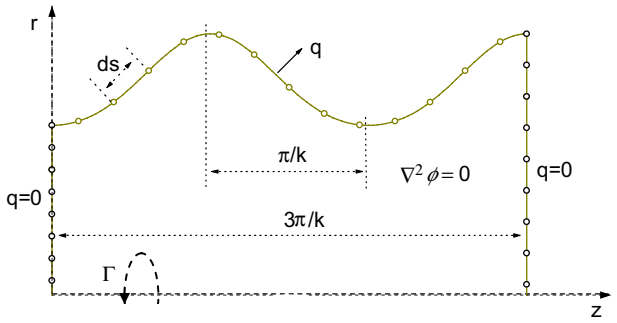

Fig. 1. Computational domain for the rotating infinite liquid jet.

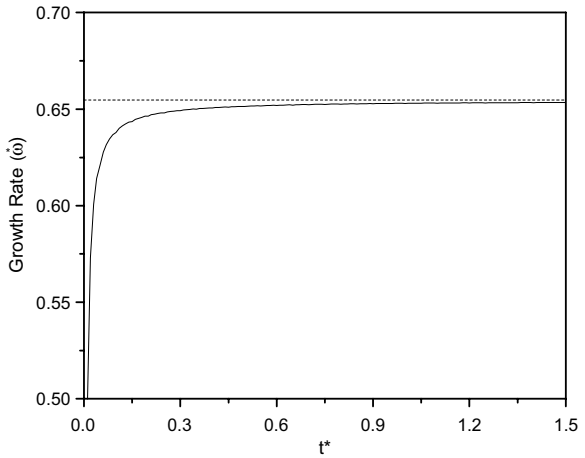

Fig. 2. Typical time history of wave growth rate ($Ro = 1.0$ and $k = 0.86$). Note that the dimensionless time, $t^* = tU_s/a$.

Fig. 3 shows a comparison of the present calculation and the result of Ponstein's linear stability analysis. This figure shows the variation of wave growth rate with wave number for the Rossby numbers of 5.0, 1.0, and 0.5. At the weakly swirled $Ro = 5$ condition, there is very little difference in the results with those computed by Rayleigh. Excellent agreement is obtained between the results of present BEM simulation and Ponstein's theoretical result for all conditions. Companion grid function convergence studies confirm the accuracy and convergence of the scheme into the nonlinear regime as well. The computational mesh spacing of $ds^* = 0.005$ was employed in subsequent calculations shown below.

3.1. Nonlinear wave forms

Using the Ponstein result in Eq. (10), one can establish the wave number that maximizes the growth rate for various levels of swirl. Using the k values resulting from this process, a series of simulations were conducted at various Ro conditions to assess the effect of swirl on nonlinear wave shapes. Figs. 4–6 summarize results from this study. Fig. 4 depicts wave shapes in the weakly nonlinear regime at various Ro conditions. The Ponstein result predicts a decrease in the most unstable wavelength as swirl is increased (Ro decreased). The $Ro = 5$ result is nearly identical to the Rayleigh jet as the results of swirl are very minimal for this condition even into the nonlinear regime.

Fig. 5 shows the breakup profiles near the pinching point for the conditions shown in Fig. 4. Here, the axial coordinate is scaled to permit all results to be presented on a column length scale from 0 to 1.0. The highly

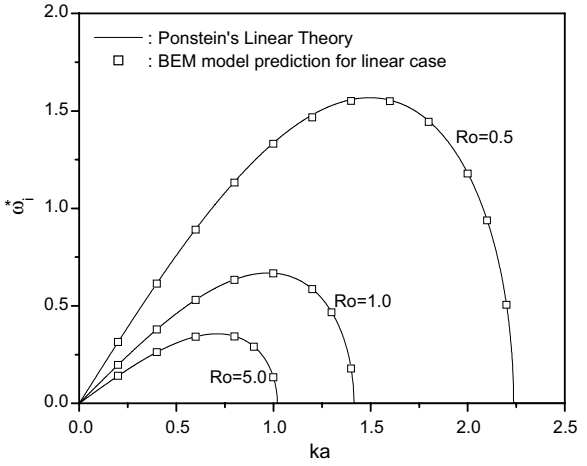

Fig. 3. Comparison of computed and theoretical growth rates for various Rossby numbers assuming an initial wave height, $\eta_0^* = 0.0001$ in the computations. Note that $Ro \geqslant 5.0$ is nearly equivalent to the Rayleigh's case, where $Ro = \infty$. The most dominant wavenumber of the Rayleigh equation, $ka = 0.7$ (equivalent wavelength is $\lambda = 9a$) is shown for the $Ro = \infty$ case.

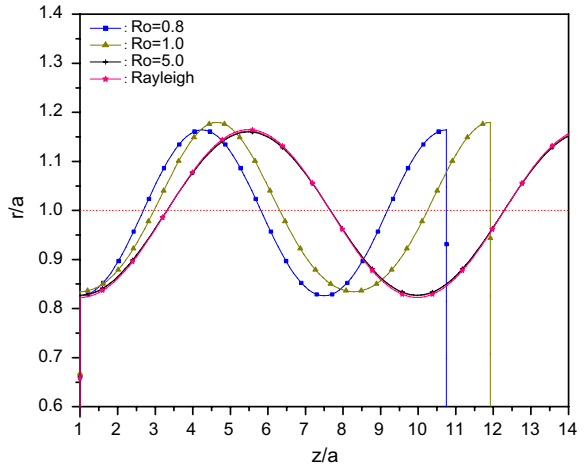

Fig. 4. Most unstable wave profiles obtained by the BEM simulation for swirling liquid jet for a variety of *Ro* values.

swirled jets tend to take on a more bulbous appearance in the main droplet, while satellite drops tend to be more flattened at this condition as compared with the weakly-swirled case. Simulations were terminated when a node on the initial jet surface came within $r/a = 0.05$ of the centerline. A similar pinch condition was utilized in prior studies (Yoon and Heister, 2004) and was shown to be sufficient for determination of droplet sizes. Since the potential vortex used to simulate swirl is singular at the centerline, the results near the pinch condition will require close scrutiny. It will be desirable to confirm the shapes with focused experiments at similar conditions.

Fig. 6 shows perspective views of the droplet formation condition at various *Ro* values. We see that the droplet shape is far from spherical at the pinchoff condition as the swirl strength is increased. The main droplet is deformed like a disk near $Ro = 0.8$ and finally it forms a doughnut shape because the droplet is stretched in the radial direction by the centrifugal force. Presumably if the swirl strength is strong enough to overcome the surface tension, the main droplet may be unstable and secondary breakup of this drop is possible. This condition was not realized under the range of *Ro* values investigated.

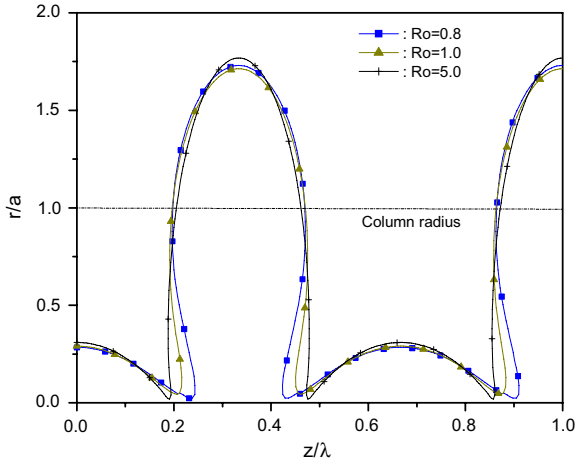

Fig. 5. Normalized wave shape (note: z/λ and r/a) for the various Rossby numbers.

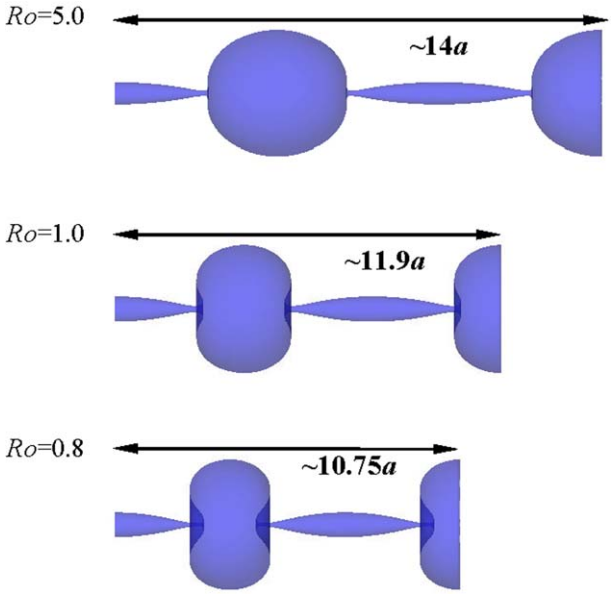

Fig. 6. Jet profiles at the pinching condition for various *Ro* values. All profiles are plotted in the same length scale.

3.2. Computed drop sizes

A series of parametric studies was conducted to illuminate the nonlinear effect of flow conditions to drop size on rotating liquid jets. Using the grids described in the previous section, typical run times for these studies were order of 1–2 h on a 1-GHz CPU computer. In order to investigate the drop size formed from the instability of rotating liquid, numerous simulations were performed at various *Ro* values for a range of wave numbers. Fig. 7 provides a summary of these studies. As with the classical Rayleigh jet, the satellite and main drops tend to merge toward a similar size at the low wavenumber, i.e. long wave, conditions. Increased swirl tends to increase the size of satellite drops relative to the unswirled conditions. By forcing the jet at a given frequency (i.e. wavenumber) and employing a given amount of swirl, a variety of bimodal distributions can be obtained.

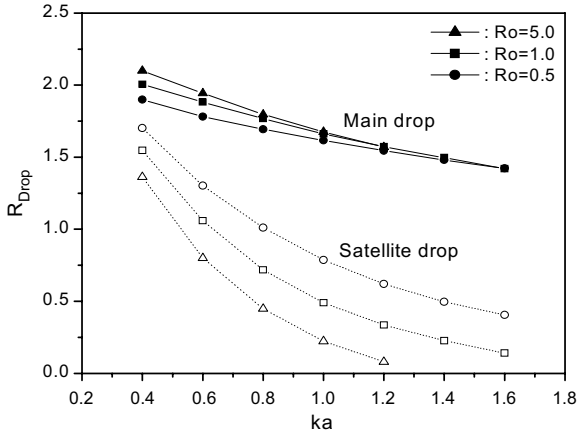

Fig. 7. Drop size as a function of wave number for various Rossby numbers. Note that the main drop radius of the nonlinear simulation is approximately ~1.87*a* while that of the linear result of the Rayleigh's prediction is ~1.89*a*. The 1.05% difference is attributed to the mass sharing with the satellite drop formed due to the nonlinearity.

Fig. 8 presents a compilation of main/satellite drop sizes assuming Ponstein's result is used to determine the k_{max} value at each *Ro*. Note here that the drop radius was calculated for perfect sphere having the corresponding volume because the drops formed are in general far from spherical as shown in Fig. 6. Both main and satellite drops tend to decrease in size under highly swirled conditions due mainly to the fact that k_{max} is increased under these conditions. The fact that the shape of the curves is nearly the same led us to investigate if there was a simple scaling between the two predicted droplet sizes.

Fig. 9 highlights the calculated droplet sizes, nondimensionalized by the Ponstein result, for various Rossby numbers. Once again, the k_{max} value from the Ponstein equation is used to predict the column length for each *Ro* condition. In Fig. 9, it is clearly shown that the ratio between main and satellite remains nearly constant even when the swirl strength was varied. It is very interesting that the ratios of these two drop sizes about the theoretical result are almost constant regardless of swirl strength. The predicted main drop size from the BEM model corresponds to 99% of theoretical result of the Ponstein equation, while the satellite drop size is 31% of the theoretical value over a large range of *Ro* values. Roughly 97% of the volume in the initial column is contained in the main drop, while the satellite drop comprises the remaining 3%. This interesting property can permit the manufacture of bimodal distributions that in principal can be quite tightly controlled.

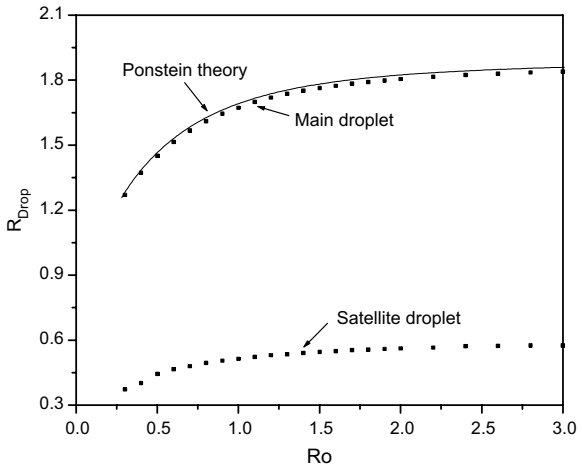

Fig. 8. Variation of predicted drop size with Rossby number assuming the most unstable wavenumber from Ponstein's equation (Eq. (10)).

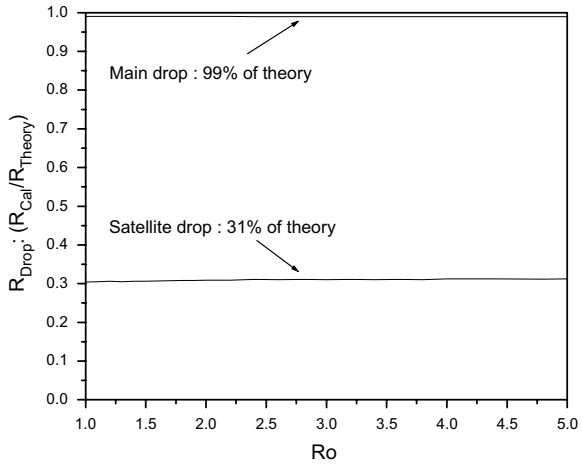

Fig. 9. The size of the main and satellite drop; it shows the ratio between the main and satellite drops as a function of the Rossby number.

Some manufacturing/printing processes further utilize electrostatics to control the paths of satellite drops and effectively sort them from the main stream. It is possible that incorporation of swirl could provide a desirable feature for controlling the satellite drop size for both forced (Fig. 7) and naturally-occurring (Figs. 8 and 9) conditions.

4. Conclusions

A fully nonlinear model has been developed for simulating the swirling jet. An axisymmetric boundary element formulation has been utilized wherein a potential vortex is superposed to the bulk flow to simulate the swirl in the jet/column. The corresponding form for the nonlinear Bernoulli equation free surface boundary condition has been developed.

A linear instability analysis due to Ponstein has been used to validate the newly developed model. The difference between computed growth rates and the theoretical results is within 1% for all conditions studied. Parametric studies were conducted while varying the swirl strength to observe their effect on the wave growth rate and drop size. Increasing swirl tends to increase the size of satellite drops and therefore provides a mechanism to control droplet sizes for low-speed liquid jets. Main drops tend to take on doughnut shapes at the pinching condition for highly swirled cases. An interesting scaling was discovered for cases where the Ponstein value of most unstable wavenumber is used at various swirling conditions. In this case, the main drop is found to be about 99% of the single drop size predicted by Ponstein, while the satellite drop is about 31% of the Ponstein drop size.

Acknowledgements

The authors greatly acknowledge the support of the Air Force Office of Scientific Research (Grant No. F49620-03-1-0025) with program manager Dr. Mitat Birkan. The second author wishes to acknowledge the partial support of this research by Carbon Dioxide Reduction & Sequestration R&D Center and by New Faculty Research Grant, funded by Korea University.

References

Hilbing, J.H., Heister, S.D., 1996. Droplet size control in liquid jet breakup. Phys. Fluids 8, 1574–1581.
Ibrahim, E.A., 1993. Effect of swirl on jet atomization. AIAA J. 31, Technical notes.
Lafrance, P., 1975. Nonlinear breakup of a laminar liquid jet. Phys. Fluids 18, 428–432.
Levich, V.G., 1962. Physicochemical Hydrodynamics. Prentice Hall, New Jersey, 639–646.

Lundgren, T.S., Mansour, N.N., 1988. Oscillations of drops in zero gravity with weak viscous effects. J. Fluid Mech. 194, 479–510.
Nayfeh, A.H., 1970. Nonlinear stability of a liquid jet. Phys. Fluids 13, 841–847.
Orme, M., Muntz, E.P., 1990. The manipulation of capillary stream breakup using amplitude-modulated disturbances: A pictorial and quantitative representation. Phys. Fluids 2, 1124–1130.
Park, H., Heister, S.D., 2006. Nonlinear simulation of free surfaces and atomization in pressure swirl atomizers. Physics of Fluids 18, 052103.
Park, H., Yoon, S.S., Heister, S.D., 2005. A nonlinear atomization model for computation of drop-size distributions and spray simulations. Int. J. Numer. Methods Fluids 48, 1219–1240.
Ponstein, J., 1959. Instability of rotating cylindrical jets. Appl. Sci. Res. 8, 425–456.
Rayleigh, W.S., 1878. On the instability of jets. Proc. London Math. Soc. 10.
Reitz, R.D., Bracco, F.V., 1982. Mechanism of atomization of a liquid jet. Phys. Fluids 25, 1730–1742.
Rutland, D.F., Jameson, G.J., 1970. Theoretical prediction of the sizes of drops formed in the breakup of capillary jets. Chem. Eng. Sci. 25, 1689–1698.
Setiawan, E.R., Heister, S.D., 1997. Nonlinear modeling of an infinite electrified jet. J. Electrostat. 42, 243–257.
Smirnov, V.I., 1964. A Course of Higher Mathematics. Pergamon Press, New York.
Spanger, C.A., Hilbing, J.H., Heister, S.D., 1995. Nonlinear modeling of jet atomization in the wind-induced regime. Phys. Fluids 7, 964–971.
Sterling, A.M., Sleicher, C.A., 1975. The instability of capillary jets. J. Fluid Mech. 68, 477–495.
Weber, C., 1931. Zum zerfall eines flussigkeitsstrahles. Z. Angew. Math. Mech. 11, 138–145.
Yoon, S.S., Heister, S.D., 2004. A nonlinear atomization model based on a boundary layer instability mechanism. Phys. Fluids 16, 47–61.
Yuen, M.C., 1968. Nonlinear capillary instability of a liquid jet. J. Fluid Mech. 33, 151–163.